# The biomechanical effects of stapes replacement by prostheses on the tympano-ossicular chain

Fernanda Gentil[1,2,3], Carolina Garbe[1], Marco Parente[1], Pedro Martins[1], Carla Santos[1], Eurico Almeida[2] and Renato Natal Jorge[1,*,†]

[1]*IDMEC, Faculdade de Engenharia da Universidade do Porto, Porto, Portugal*
[2]*Clínica ORL – Dr. Eurico Almeida, Porto, Portugal*
[3]*Widex, ESTSP, Portugal*

SUMMARY

Hearing is a sequence of processes in which the ear translates sound waves into electrical signals, which are then sent to the brain where they are interpreted as sound. The ossicular chain of the middle ear is formed by three ossicles (malleus, incus, and stapes), of which the last and smallest, the stapes, vibrates, thus communicating with the inner ear through the stapes footplate. When abnormal bone formation immobilizes the stapes (otosclerosis), the passage of sound does not correctly occur and hearing can be compromised. In most cases, surgery is an option for its treatment. The stapes is totally or partially replaced by a prosthesis (stapedectomy or stapedotomy, respectively) allowing the passage of sound to the inner ear.

This work presents a study on the behavior of different stapes prostheses, considering their biomechanical characteristics. The stapes was replaced by different prostheses, made of dissimilar materials: stainless steel, teflon, and titanium. The umbo and stapes footplate displacements for the models with these prostheses were obtained and compared with the displacements obtained with the model representative of the normal ear.

In the models with prostheses, the displacements are found in the hole where the prosthesis is attached.

KEY WORDS: biomechanics; stapes; prostheses; FEM

## 1. INTRODUCTION

The middle ear is a closed, air-filled chamber, separated from the external ear by the eardrum, and ventilated by the Eustachian tube. The stapes, the smallest bone in the human body, comes third in the tympano-ossicular chain of the middle ear. Its height can be of about 4.5 mm, the average being 3.26 mm and weights approximately 2 mg (Figure 1). The other bones are the malleus and the incus [1]. It is through the stapes and the stapes footplate that the connection between the middle ear and the inner ear occurs [2].

The human ear converts sound energy into mechanical energy and then into nerve impulses transmitted to the brain. When the vibration of the stapes does not render correctly because of the overgrowth of bone (otosclerosis), conductive hearing loss is experienced. Sometimes, otosclerosis spreads to the inner ear, and then, a sensorineural hearing impairment may result because of the interference with the nerve function. This impairment is called cochlear otosclerosis, and it may be permanent. On occasion, the otosclerosis may spread to the semicircular canals and may cause episodes of balance disorders.

Figure 1. Close-up view of a human stapes.

The fixation of the stapes was first described by Valsalva in 1704 during an autopsy. On microscopic evidence of 1890, Katz showed this disease as otosclerosis. In 1893, Politzer described it as a 'primary metabolic bone disease of otic capsule'. The hearing loss resulting of otosclerosis can be corrected by hearing aids, but the most appropriate treatment is surgery, which consists in the removal of the suprastructure of the stapes (stapedotomy) then drilling a hole into the footplate and inserting a piston prosthesis, or the entire stapes (stapedectomy), and its replacement by a prosthesis fixed at the long crus of the incus.

The first document, about surgical technique for stapes mobilization, date back to 1876 with a description of mobilization of the stapes footplate. The world's first stapedectomy has been credited to Dr. John J. Shea, Jr., who performed it in May, 1956, on a 54-year-old housewife who could no longer hear even with a hearing aid. The surgery included the removal of the stapes covering the oval window with a vein graft and the insertion of a nylon prosthesis from the incus to the oval window [3, 4]. John House described a technique that allows to avoid a direct drilling on the oval window. Many of these developed techniques are still used today with few variations, respecting the basic principle of allowing the connection between the eardrum and the vestibule [5].

There are two major causes of stapes fixation, otosclerosis and congenital malformation of the stapes. In both situations, it is possible to improve hearing by either removing the stapes entirely (stapedectomy) or partially (stapedotomy) [6]. This procedure greatly reduces the chance of a perilymph fistula (leakage of cochlear fluid) and can be further improved by the use of a tissue graft seal of the oval window [7, 8]. The hole diameter can be predetermined according to the prosthesis diameter. The results of this surgery are generally most reliable in patients whose stapes has lost mobility because of otosclerosis. Successful surgery usually provides an increase in hearing ability of about 20 dB. However, most of the published results of success fall within the speech frequency of 500, 1, and 2 kHz with poor results in the high frequency domain [9].

Among some procedures, the main steps of the surgery are shown in Figure 2. The stapes, attached to the incus, is separated (Figure 2(a)). The stapes suprastructure is then 'downfractured' leaving the footplate still within the oval window (Figure 2(b)). A laser or drill is used to make a small hole in the footplate (Figure 2(c)). The prosthesis is placed over the incus and into the hole in the footplate (Figure 2(d)).

Over time, various materials, such as stainless steel, teflon-type polymer, titanium, gold, platinum, and others, have been used to manufacture prostheses and so have there been variations in size, shape, weight, and mass. The main differences in the design of stapes prostheses are focused on both ends allowing for a good fixation of the prosthesis with the incus, as well as ways to improve the transmission of sound through the oval window to the inner ear [10].

Titanium prostheses represent the latest development in the field of all-metal prostheses. Titanium is known for its particularly good biocompatibility also ensuring MRI compatibility. The physical parameters that influence sound transmission include density and stiffness.

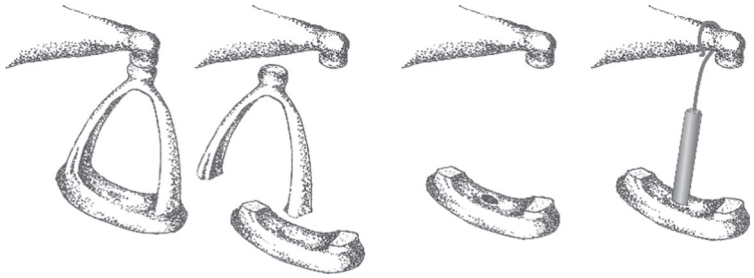


Figure 2. The main steps of stapedotomy.

The audiogram, tympanometry, and acoustic reflexes are the most important objective audiological exams in the diagnosis of otosclerosis.

The bulk of current work is directed toward the geometrical design and material selection of prostheses. Replacing the stapes of the middle ear is a challenging problem because of size constraints and the need for an adequate prosthesis. Finite element models can be used to test (in a numerical simulation) prostheses with different designs and sizes. Detailed geometrical models of the eardrum and tympano-ossicular chain of the middle ear were obtained from high-resolution computerized tomography (CT) image sets. In order to develop models to optimize the prostheses, it is important to understand the biomechanics of hearing in the diseased ear, to improve rehabilitation methods in patients suffering from otosclerosis.

The first known work, about the biomechanical behavior of the middle ear, using the FEM, was carried out on a cat and dates back from 1978 [11]. Other models from the geometry of the human middle ear have been developed, considering the eardrum, the ossicles, and cochlear impedance, including the insertion of some ligaments and tendons [12–16]. Some of these works compare their results with experimental data. The displacements obtained at the umbo and the stapes footplate were compared with other existing numerical and experimental studies in literature [17–22]. The new insights the construction of this model were the contact formulation for the simulation of capsular ligaments, the ligaments considered with hyperelastic behavior, the command tie for the connection between the prosthesis and the incus, and the constitutive model used for simulating the passive function of the muscles in the middle ear.

The aim of this study is to numerically simulate, using the the FEM, the biomechanical effects of stapes replacement by prostheses on the tympano-ossicular chain made from different materials, such as stainless steel, teflon, and titanium, comparing the obtained results with those from a simulation of the representative normal ear model.

## 2. MATERIALS AND METHODS

The first step of this work was the construction of the tympano-ossicular chain model of the middle ear (eardrum and the three ossicles, malleus, incus, and stapes) including ligaments (superior, lateral, and anterior of the malleus, superior and posterior of the incus, annular ligament of the stapes) and two muscles (tensor tympani and stapedius). The geometrical construction of the bones was mainly on the basis of CT images [23]. The images were obtained from a 65-year-old woman , with no ear pathology. For more details of the model, please consult the reference [24]. The geometry was obtained from slices 0.5 mm thick. The finite element software ABAQUS was used to handle the numerical simulations [25].

Because of the reduced dimensions of the stapes, the details captured on the CT images were not sufficient; therefore, the stapes was constructed using anatomical bibliographic information [26], and a manual procedure was used, by using a CAD software [27, 28].

The height and width of the eardrum are, respectively, 11 and 9 mm, and its thickness is 0.1 mm, on the basis of references [13, 29, 30]; the malleus height is 8.5 mm and the incus 7 mm; the stapes measures 3.3 mm.

The eardrum was modeled with hexahedral elements (ABAQUS C3D8 element). It was divided into *pars flaccida*, considered as isotropic (with only one layer), and *pars tensa* (with three layers). The internal and external layers were considered isotropic, and the middle one, fibrous, was considered orthotropic [31]. For the ossicles, tetrahedral elements with four nodes were used (ABAQUS C3D4 element), assuming an isotropic behavior, and with elastic properties obtained from the literature [16]. The ligaments and muscles were modeled using linear elements of type T3D2. For the ligaments, the present study used a hyperelastic nonlinear behavior, on the basis of the Yeoh constitutive model [32–35]. Yeoh model is a polynomial form of the strain energy function that depends on the strain invariant $I_1$. It was first applied to model the behavior of carbon black-filled rubber. It is suitable to represent the nonlinear behavior of incompressible materials such as rubber or highly hydrated soft tissues and available in commercial FE software packages such as ABAQUS [25].

For the muscles, the Hill constitutive model was used [36, 37].

The simulation of the cochlear fluid is modeled with fluid elements, of type F3D3, assuming an incompressible behavior.

The connection between the malleus and the incus, simulating the incudomalleolar joint, is conducted by using contact formulation. The basic Coulomb friction model available in the ABAQUS software is used [25]; the friction rate was set to 0.7 [38].

Boundary conditions for the finite element model include the *pars tensa* of the eardrum periphery to simulate the tympanic annulus; the connection between the stapes footplate and the cochlea, to simulate the stapes annular ligament; the connection of suspensory ligaments (superior, lateral, and anterior of the malleus and superior and posterior of the incus); and the muscles (tensor tympani and stapedius) to the tympanic cavity walls.

In order to numerically simulate the effect of the different prostheses, two 3D solid models were created, according to the shapes and sizes of the prostheses models (Figure 3).

The materials considered throughout the numerical simulation include stainless steel, teflon, and titanium. The discretization of these prostheses was carried out by using the FEM (C3D4 element). Figure 4 shows the finite element meshes used for the three prostheses. The stainless steel and titanium prostheses were assumed as being of the same shape.

The respective material properties are shown in Table I. For the connection between the prosthesis and the incus, throughout the numerical simulations, the nodes from the prosthesis were considered to have been tied (using the command tie in ABAQUS software) [25]. For the connection between the prosthesis and the stapes footplate, a hole with the dimensions and direction of the prosthesis

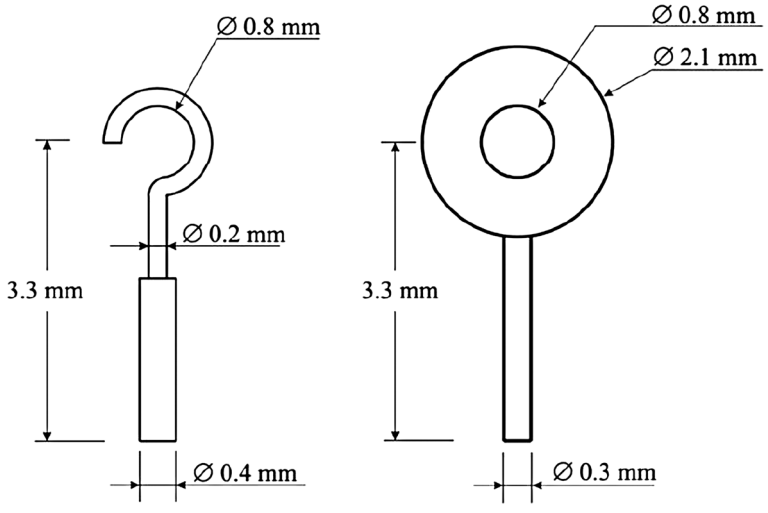


Figure 3. Dimensions and geometry of the prostheses considered.

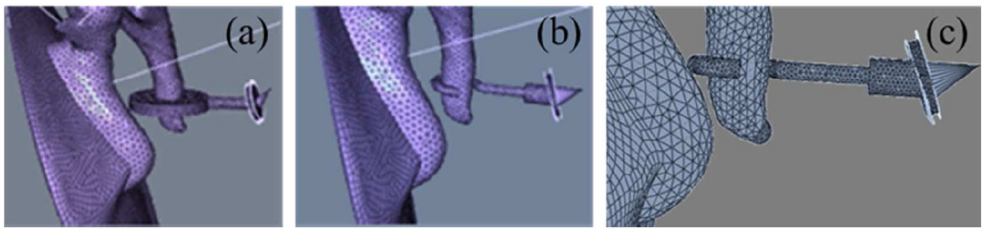


Figure 4. Finite element meshes for (a) teflon, (b) stainless steel, and (c) titanium prostheses.

Table I. Material properties for the prostheses.

| Material | Young's modulus $\left(N/m^2\right)$ | Poisson's ratio | Density $\left(\mathrm{kg/m^3}\right)$ | References |
|---|---|---|---|---|
| Stainless steel | 2.10 E + 11 | 0.30 | 7.80 E + 03 | [39] |
| Teflon | 6.00 E + 08 | 0.44 | 2.20 E + 03 | [40] |
| Titanium | 1.14 E + 11 | 0.34 | 4.43 E + 03 | [41] |

piston was performed on the stapes footplate. The nodes of the piston were constrained in order to allow only piston-like movements.

The constitutive equation adopted in this work for the 3D passive behavior of the muscles is based on previous works of the authors [42, 43] and is a modified form of the incompressible, transversely isotropic, hyperelastic model proposed by Humphrey and Yin [44] for passive cardiac tissues.

For the constitutive model used, the strain energy per unit volume of the reference configuration can be written, for the general 3D case, in the following form [43]:

$$U = U_I\left(\bar{I}_1^C\right) + U_f\left(\bar{\lambda}\right) + U_J\left(J\right) \tag{1}$$

In (1), $U_I$ is the strain energy stored in the isotropic matrix, embedding the muscle fibers, and $U_f$ is the strain energy stored in each muscle fiber:

$$U_I\left(\bar{I}_1^C\right) = c\left\{\exp\left[b\left(\bar{I}_1^C - 3\right)\right] - 1\right\}, \tag{2}$$

$$U_f\left(\bar{\lambda}_f\right) = A\left\{\exp\left[a\left(\bar{\lambda}_f - 3\right)^2\right] - 1\right\} \tag{3}$$

In (2) and (3), $\bar{I}_1^C$ is the first invariant of the right Cauchy–Green strain tensor whose volume change has been eliminated:

$$\bar{I}_1^C = \mathrm{tr}\,\bar{\mathbf{C}} = \mathrm{tr}\,\left(\bar{\mathbf{F}}^T\bar{\mathbf{F}}\right) = J^{-\frac{2}{3}}\mathrm{tr}\,\mathbf{C}, \tag{4}$$

In (4) $J$, the jacobian determinant, representing the ratio of volume before and after deformation, caused by a given deformation gradient and is obtained as follows:

$$J = \det\,\mathbf{F}, \tag{5}$$

and $\bar{\lambda}_f$ is the fiber stretch ratio in the direction $\mathbf{N}$ of the undeformed fiber, given by the following:

$$\bar{\lambda}_f = \sqrt{\mathbf{N}^T\bar{\mathbf{C}}N} = \sqrt{\bar{\mathbf{C}} : (\mathbf{N}\otimes\mathbf{N})} \tag{6}$$

were $\otimes$ denotes the tensor product. When $\bar{\lambda}_f < 1$, we consider the strain energy $U_f$ to be zero, assuming that the muscle fibers offer no resistance to compression.

In (1), $U_J$ is responsible for ensuring the incompressibility condition and is defined by the following:

$$U_J = \frac{1}{D}\left(J-1\right)^2 \tag{7}$$

In these definitions, the constitutive parameters of the constants [43] are $c$ = 1.85 E − 2 N/mm$^2$, $b$ = 1.173; $A$ = 2.80 E − 2 N/mm$^2$, a = 0.6215, and $D$ = 1 E − 4 mm$^2$/N.

The strain energy density given in (1) is now used to obtain the second Piola–Kirchhoff stress tensor **S**:

$$\mathbf{S} = \frac{\partial U}{\partial \mathbf{E}} = \frac{\partial U_I}{\partial \mathbf{E}} + \frac{\partial U_f}{\partial \mathbf{E}} + \frac{\partial U_J}{\partial \mathbf{E}} \tag{8}$$

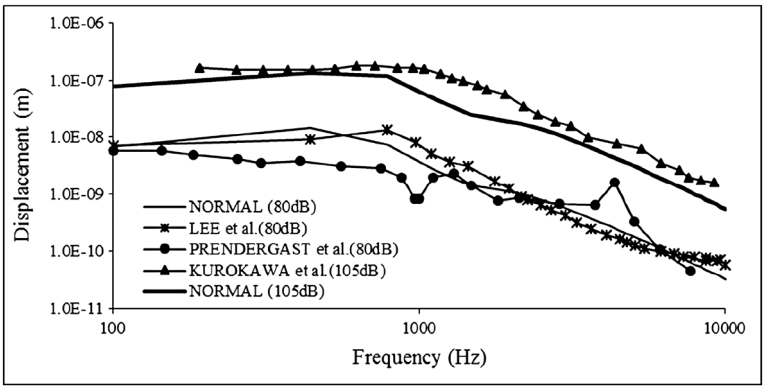


Figure 5. Stapes footplate displacement for 80 and 105 dB sound pressure level applied to the eardrum.

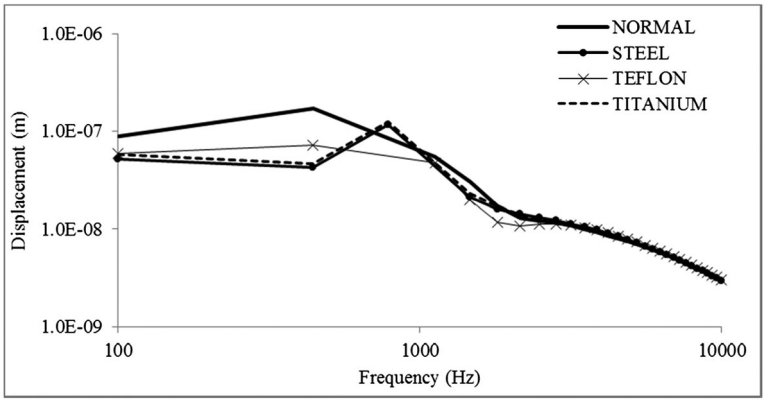


Figure 6. Umbo displacement, for 90 dB sound pressure level applied to the eardrum.

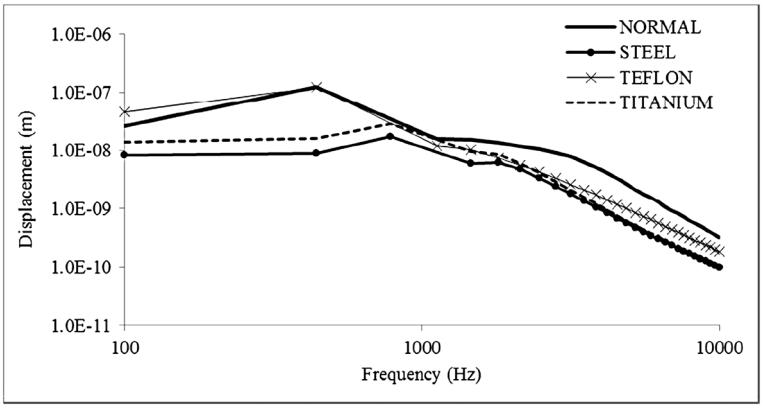


Figure 7. Stapes footplate displacement, for 90 dB sound pressure level applied to the eardrum.

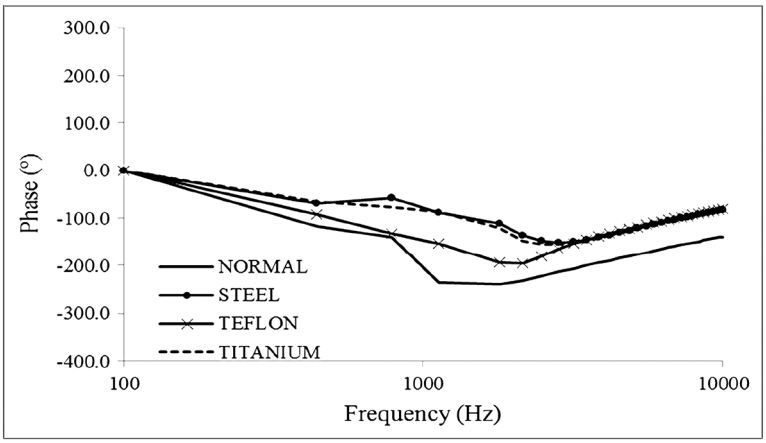


Figure 8. Corresponding phase angles of the umbo.

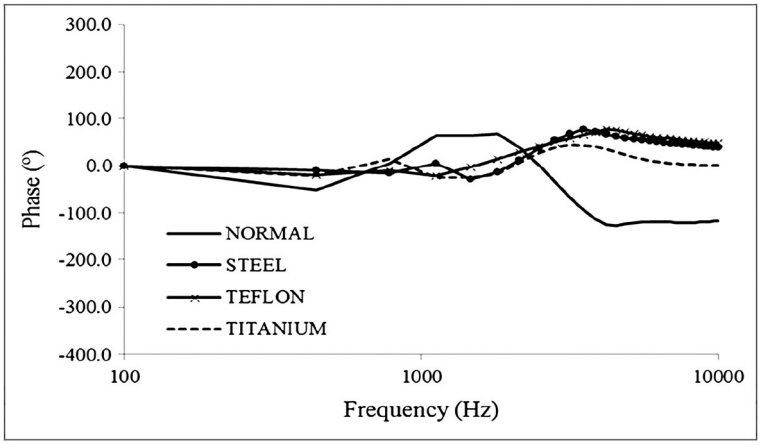


Figure 9. Corresponding phase angles of the stapes footplate.

The Cauchy stress tensor $\boldsymbol{\sigma}$ is related to the second Piola–Kirchhoff stress tensor $\mathbf{S}$ by the following:

$$\boldsymbol{\sigma} = \frac{1}{J}\mathbf{F}\mathbf{S}\mathbf{F}^{T} \tag{9}$$

The material version of the tangent operator $\mathbf{H}$, which is necessary for the implementation of the constitutive model in ABAQUS, is defined as follows:

$$\mathbf{H} = \frac{\partial^2 U}{\partial \mathbf{E} \partial \mathbf{E}} = \frac{\partial \mathbf{S}}{\partial \mathbf{E}} \tag{10}$$

Using a push-forward operation, which transforms a vector or tensor-valued quantity on the basis of the reference (material) configuration to the current (spatial) configuration, the spatial tangent operator $\mathbf{h}$ can now be obtained:

$$\mathbf{h}_{ijkl} = \frac{1}{J} F_{im} F_{jn} F_{kp} F_{lq} H_{mnpq} \tag{11}$$

Because the proposed constitutive model was used in ABAQUS with 1D finite elements, (T3D2 beams), some modifications can be applied, as shown in the Appendix.

## 3. RESULTS

In order to validate the model created for the normal tympano-ossicular chain, a dynamic study was conducted for a frequency range between 100 and 10 kHz. The amplitude of the sound pressure of 0.2 and 3.557 Pa was applied to the eardrum, which corresponds respectively to 80 dB sound pressure level (SPL) and 105 dB SPL. For 80 dB SPL, the results were compared with the experimental results obtained by Lee *et al*. [18] and computational results of Prendergast *et al*. [16]. For 105 dB SPL, the results were compared with the experimental study of Kurokawa [45]. Figure 5 shows the stapes footplate displacements, which are in accordance with the results obtained by the different authors.

For the study on the prosthesis effect, a sound pressure level of 90 dB SPL (0.63 Pa) was applied to the eardrum, and a dynamic study was made for the same frequency range (100–10 kHz). The displacements obtained for the umbo (central part of the eardrum at the end of the malleus) were compared between the three different prostheses and with the results obtained from the representative model of the normal tympano-ossicular chain (Figure 6).

It can be observed that for the highest and medium frequencies that the displacements are equivalent. For the low frequencies, all displacements are smaller when compared with the normal model, being the nearest results obtained those with the teflon prosthesis.

The displacements obtained from the central part of the stapes footplate were compared between the normal model and the models with three different prostheses, which are shown in Figure 7. When the stapes is replaced by a steel or titanium prostheses, the displacements have lower values along the entire frequency range. Teflon is the material that is the the closest to the normal ear model, especially at lower frequencies.

Figures 8 and 9 show the corresponding phase angles of the umbo and stapes footplate, respectively. From the graph presented in Figure 8, one can see that the values obtained for the normal model are lower than the results of the prostheses, showing no significant differences between prostheses for higher frequencies. For the stapes footplate (Figure 9), at higher frequencies, the results for the normal model are lower than the ones obtained with the prostheses; however, they are slightly higher at middle frequencies.

Figure 10 shows the velocity measured at the central part of the stapes footplate, for the normal model of the ossicular chain and for the models with prostheses. The model with the teflon prosthesis shows close results with the normal model, at lower frequencies. All models with prosthesis showed lower velocities at higher frequencies and were in good agreement at frequencies around 3 kHz, when compared with the normal model.

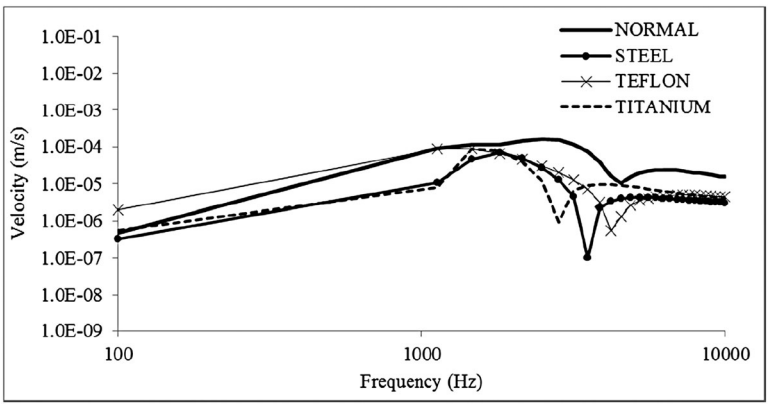


Figure 10. Velocity at the central part of the stapes footplate.

## 4. CONCLUSIONS

Nowadays, although otosclerosis is considered to be one of the best known causes for hearing loss, it still remains a field for surgical improvement. The complete understanding of otosclerosis remains a challenge for the scientific community. Despite the effort for introducing several alternative therapeutical options, otosclerosis management is undoubtedly surgical, with stapedectomy being considered the best surgical option. The introduction of new materials in stapes prostheses has given surgeons the opportunity to diminish the duration and technical difficulties of the surgery. Improvements of the stapes prostheses can offer significant advantages and better audiological results, with the absence of major postoperative complications.

To compare the effectiveness of two stapes prostheses (titanium versus teflon) in hearing improvement of patients undergoing stapes surgery for otosclerosis, both prostheses provided comparable results, although the teflon platinum wire prosthesis was slightly superior [46].

The objective of the study published by Lippy *et al*. [47] was to determine whether a titanium piston stapes prosthesis would be audiometrically and surgically equivalent to a Robinson stainless steel piston for stapedectomy. The authors conclude that titanium stapes prosthesis is a good alternative to a stainless steel prosthesis.

Another study by Cotulbea *et al*. [48] presents an experience with the Fisch-type 0.4 mm titanium prosthesis that was compared with the hearing results obtained with two types of prostheses (Causse-type teflon pistons and stainless steel pistons). Although the functional results of the three different types of stapes prosthesis did not vary significantly, the Fisch-type 0.4 mm titanium piston gave a somewhat better result in closing the air-bone gap in the 10 dB range. This may be due to a better fixation of the prosthesis to the long process of the incus. The good characteristics of the titanium piston made it the first choice in stapes surgery, gradually replacing the other two types of stapes prostheses. A comparison of these and our results has evidenced that the 0.4 mm model may provide better results than the 0.8 mm model.

In this study, in the higher frequencies, from the numerical point of view, there are no significant differences. It is in the lower frequencies that major differences between materials are revealed. Comparing the mass of the four materials (bone = 1.78 mg; teflon = 1.93 mg; steel = 1.50 mg, and titanium = 0.85 mg) and their respective Young's modulus (Table I), one can verify that the prosthesis of teflon is the one whose properties are the most approximate to those of the bone.

A conclusion of this study is the adequacy of the teflon prosthesis as a replacement for the stapes. The matching between the results of the model representative of normal ear and those of the ear model with the prosthesis in teflon is especially evident at lower frequencies. This result may be because of the lower stiffness and density of teflon when compared with stainless steel and titanium.

## APPENDIX

On the present work, the proposed constitutive model for the muscles behavior was used with 1D beam elements (ABAQUS T3D2 beam element). Because these elements fully respect the incompressibility condition, some modifications can be applied in the user subroutine (ABAQUS UMAT) [25]. In order to ensure the incompressibility condition $J = 1$, the deformation gradient $\mathbf{F}$ and the right Cauchy–Green strain tensor $\mathbf{C}$ become the following:

$$\mathbf{F} = \begin{pmatrix} \lambda & 0 & 0 \\ 0 & \frac{1}{\sqrt{\lambda}} & 0 \\ 0 & 0 & \frac{1}{\sqrt{\lambda}} \end{pmatrix}; \quad \mathbf{C} = \mathbf{F}^T\mathbf{F} = \begin{pmatrix} \lambda^2 & 0 & 0 \\ 0 & \frac{1}{\lambda} & 0 \\ 0 & 0 & \frac{1}{\lambda} \end{pmatrix} \tag{A.1}$$

Because $J = 1$, the following simplifications are obtained: $\mathbf{C} = \bar{\mathbf{C}}$, $\bar{I}_1^C = I_1^C$, and $\bar{\lambda}_f = \lambda$.

The strain energy density given in (1) is now used to obtain the second Piola–Kirchhoff stress tensor $\mathbf{S}$:

$$\mathbf{S} = \frac{\partial U}{\partial \mathbf{E}} = \frac{\partial U_I}{\partial \mathbf{E}} + \frac{\partial U_f}{\partial \mathbf{E}} \tag{A.2}$$

The derivatives $\frac{\partial U_I}{\partial \mathbf{E}}$ and $\frac{\partial U_f}{\partial \mathbf{E}}$ are obtained as follows:

$$\frac{\partial U_I}{\partial \mathbf{E}} = \frac{\partial U_I}{\partial I_1^C} \frac{\partial I_1^C}{\partial \mathbf{E}} \tag{A.3}$$

$$\frac{\partial U_f}{\partial \mathbf{E}} = \frac{\partial U_f}{\partial \lambda} \frac{\partial \lambda}{\partial \mathbf{E}} \tag{A.4}$$

with

$$\frac{\partial I_1^C}{\partial \mathbf{E}} = 2\mathbf{I} \tag{A.5}$$

where $\mathbf{I}$ is the unit second order tensor, and

$$\frac{\partial \lambda}{\partial \mathbf{E}} = \frac{1}{\lambda} \mathbf{N} \otimes \mathbf{N} \tag{A.6}$$

$$\frac{\partial U_I}{\partial I_1^C} = bc \exp\left[b\left(I_1^C - 3\right)\right] \tag{A.7}$$

$$\frac{\partial U_f}{\partial \lambda} = 2a\left(\lambda - 1\right) A \exp\left[a\left(\lambda - 1\right)^2\right] \tag{A.8}$$

For the 1D finite element, only the tension along the beam direction is obtained. In the end, the final expression for the Cauchy stress along the beam direction is as follows:

$$\sigma = \frac{4}{3}\left(\lambda^2 - \lambda^{-1}\right) bc \exp\left[b\left(\lambda^2 + 2\lambda^{-1} - 3\right)\right] + \frac{4}{3}\lambda A a\left(\lambda - 1\right) \exp\left[a\left(\lambda - 1\right)^2\right] \tag{A.9}$$

In the case of 1D finite elements, $h$ is reduced to a constant:

$$h = \frac{4}{9}\left(\lambda^2 + 5\lambda^{-2}\right) \frac{\partial U_I}{\partial I_1^C} + \frac{16}{9}\left(\lambda^4 - 2 + \lambda^{-4}\right) \frac{\partial^2 U_I}{\partial I_1^C \partial I_1^C} - \frac{2}{9}\lambda \frac{\partial U_f}{\partial \lambda} + \frac{4}{9}\lambda^2 \frac{\partial^2 U_f}{\partial \lambda \partial \lambda} \tag{A.10}$$

Replacing the following derivatives in (A.10):

$$\frac{\partial^2 U_I}{\partial I_1^C \partial I_1^C} = b^2 c \exp\left[b\left(I_1^C - 3\right)\right] \tag{A.11}$$

$$\frac{\partial^2 U_f}{\partial \lambda \partial \lambda} = 2aA \exp\left[a\left(\lambda - 1\right)^2\right]\left[1 + 2a\left(\lambda - 1\right)^2\right] \tag{A.12}$$

The final expression for $h$ can be obtained as follows:

$$\begin{aligned} h = {} & \frac{4}{9}\left(\lambda^2 + 5\lambda^{-2}\right) bc \exp\left[b\left(I_1^C - 3\right)\right] + \frac{16}{9}\left(\lambda^4 - 2 + \lambda^{-4}\right) b^2 c \exp\left[b\left(I_1^C - 3\right)\right] \\ & - \frac{4}{9}\lambda a\left(\lambda - 1\right) A \exp\left[a\left(\lambda - 1\right)^2\right] + \frac{8}{9}\lambda^2 aA \exp\left[a\left(\lambda - 1\right)^2\right]\left[1 + 2a\left(\lambda - 1\right)^2\right]. \end{aligned} \tag{A.13}$$

ACKNOWLEDGEMENTS

The authors would like to thank the Ministério da Ciência, Tecnologia e Ensino Superior – Fundação para a Ciência e a Tecnologia in Portugal and by FEDER for the funding provide under the research project 'Estudo bio-computacional do zumbido' with the reference PTDC/SAU-BEB/104992/2008 and fellowship SFRH/BPD/71080/2010.

The authors would also like to thank J. Belinha for the collaboration provided in drawing Figure 2.

REFERENCES

1. Paparella MM, Shumrick DA. *Otorrinolaringologia* (2ª edn). Editora Médica Panamericana SA: Buenos Aires, 1982; 196–212.
2. Anson B, Donaldson J. The surgical anatomy of the temporal bone and ear, 1976.
3. Glasscock ME, Storper IS, Haynes DS, Bohrer PS. Twenty-five years of experience with stapedectomy. *Laryngoscope* 1995; **105**:899–904.
4. Shea JJ Jr. Fenestration of the oval window. *Annals of Otology Rhinology* 1958; **67**:932–951.
5. Velegrakis GA. Otosclerosis: state of the art. *Otorhinolaryngologia - Head and Neck Surgery Issue* 2011; **43**:6–16.
6. Fisch U. Commentary – stapedotomy versus stapedectomy. *Otology & Neurotology* 2009; **30**(8):1166–1167.
7. Paum PB, Pollak AM, Fisch U. Utricle, saccule and cochlear duct in relation to stapedotomy: A histologic temporal bone study. *Ann Oto Rhinol Laryngol* 1991; **100**(12):966–970.
8. Souza C, Glasscock ME. Otosclerosis and stapedectomy: diagnosis, management & complications, Thieme, 2004.
9. Raman R. Poor high frequency results following total stapedectomy theoretical considerations. *Indian Journal of Otolaryngology and Head & Neck Surgery* 1983; **35**(1):9–11.
10. Tange RA, Grolman W, Dreschler WA. Gold and titanium in the oval window: a comparison of two metal stapes prostheses. *Otology & Neurotology* 2004; **25**(2):102–105.
11. Funnell WRJ, Laszlo CA. Modeling of the cat eardrum as a thin shell using the finite element method. *Journal of the Acoustical Society of America* 1978; **63**:1461–1467.
12. Wada H, Metoki T, Kobayashi T. Three-dimensional finite-element method (FEM) analysis of the human middle ear. In *Middle Ear Mechanics in Research and Otosurgery*, Hüttenbrink KB (ed.). Department of Oto-Rhino-Laryngology, 1996; 76–80.
13. Koike T, Wada H, Kobayashi T. Modeling of the human middle ear using the finite element method. *Journal of the Acoustical Society of America* 2002; **111**(3):1306–1317.
14. Williams KR, Blayney AW, Rice HJ. Development of a finite element model of the middle ear. *Revue de Laryngologie-Otologie-Rhinologie* 1996; **117**:259–264.
15. Beer HJ, Bornitz M, Hardtke HJ, Schmidt R, Hofmann R, Vogel U, Zahnert T, Hüttenbrink HKB. Modelling of components of the human middle ear and simulation of their dynamic behavior. *Audiol. Neurootol.* 1999; **4**:156–162.
16. Prendergast PJ, Ferris P, Rice HJ, Blayney AW. Vibro-acoustic modelling of the outer and middle ear using the finite-element method. *Audiology & Neuro-Otology* 1999; **4**:185–191.
17. Ferris P, Prendergast PJ. Middle-ear dynamics before and after ossicular replacement. *Journal of Biomechanics* 2000; **33**:581–590.
18. Lee CF, Chen PR, Lee WJ, Chen JH, Liu TC. Computer aided three-dimensional reconstruction and modeling of middle ear biomechanics by high-resolution computed tomography and finite element analysis. *Biomedical Engineering-Applications, Basis & Communications* 2006; **18**(5):214–221.
19. Nishihara S, Goode RL. Measurement of tympanic membrane vibration in 99 human ears. In *Middle Ear Mechanics in Research and Otosurgery*, Hüttenbrink KB (ed.). Dresden University of Technology: Dresden, Germany, 1996; 91–93.
20. Huber A, Ball G, Asai M, Goode R. *The Vibration Pattern of the Tympanic Membrane After Placement of a Total Ossicular Replacement Prosthesis*: Dresden, Germany, 1997.
21. Gan RZ, Sun Q, Robert KD Jr., Chang KH, Dormer KJ. Three-dimensional modeling of middle ear biomechanics and its applications. *Otol and Neurotol* 2002; **23**(3):271–280.
22. Sun Q, Gan RZ, Chang KH, Dormer KJ. Computer-integrated finite element modeling of human middle ear. *Biomechanics and Modeling in Mechanobiology* 2002; **1**(2):109–122.
23. Gentil F, Jorge RN, Parente MPL, Martins PALS, Ferreira AJM. Estudo biomecânico do ouvido médio. *Clínica e Investigação em Otorrinolaringologia* 2009; **3**(1):24–30.
24. Gentil F, Garbe C, Parente M, Martins P, Ferreira A, Natal R, Santos C, Paço J. Analysis of eardrum pathologies using the finite element method. *Journal of Mechanics in Medicine and Biology* 2014; **14**(3):1450034 (20 pages).
25. Hibbit D, Karlsson B, Sorenson P. *ABAQUS Analysis User's Manual, Version 6.5*. Hibbit, Karlsson & Sorenson Inc.: USA, 2004.
26. Sanna M, Russo A, Donato GD. *Color Atlas of Otoscopy – From Diagnosis to Surgery*. Thieme: Stuttgart, New York, 1999.
27. Alexandre F, Fernandes AA, Jorge RN, Gentil F, Martins P, Mascarenhas T, Milheiro C, Ferreira AJM, Parente MPL. 3D reconstruction of the middle ear for FEM simulation. In *Computational Modelling of Objects Represented*

*in Images: Fundamentals, Methods and Applications*, Tavares JMRS, Natal Jorge RM (eds). Simpósio Internacional CompIMAGE -: Coimbra, 2006; 181–184.
28. Alexandre F, Jorge RN, Tavares JM, Mascarenhas T, El Sayed RF, Fernandes AA, Gentil F, Ferreira AJM. *Segmentação e Reconstrução 3D de Estruturas em Imagens Médicas-Comparação Entre Uma Metodologia Automática e Uma Outra Manual*. CMNE/CILAMCE: Porto, 2007.
29. Gan RZ, Feng B, Sun Q. Three-dimensional finite element modeling of human ear for sound transmission. *Annals of Biomedical Engineering* 2004; **32**(6):847–859.
30. Wever EG, Lawrence M. *Physiological Acoustics*. Princeton University Press: Princeton, 1954.
31. Garbe C, Gentil F, Parente M, Martins P, Jorge RN. Aplicação do método dos elementos finitos no estudo da membrana timpânica. *Audiologia Em Revista* 2009; **II**(3):99–106.
32. Yeoh OH. Characterization of elastic properties of carbon-black-filled rubber vulcanizates. *Rubber Chemistry and Technology* 1990; **63**:792–805.
33. Gentil F, Jorge RMN, Ferreira AJM, Parente MPL, Martins PALS, Almeida E. Biomechanical simulation of middle ear using hyperelastic models. *Journal of Biomechanics* 2006; **39**(1):388–389.
34. Martins PALS, Jorge RMN, Ferreira AJM. A comparative study of several material models for prediction of hyperelastic properties: application to silicone-rubber and soft tissues. *Strain* 2006; **42**:135–147.
35. Gentil F, Parente M, Martins P, Garbe C, Jorge RN, Ferreira A, Tavares JMRS. The influence of mechanical behaviour of the middle ear ligaments: a finite element analysis. *Journal of Engineering in Medicine* 2011; **225**(1):68–76.
36. Martins JAC, Pires EB, Salvado R, Dinis PB. A numerical model of passive and active behavior of skeletal muscles. *Computer methods in applied mechanics and engineering* 1998; **151**:419–433.
37. Gentil F, Parente M, Martins P, Garbe C, Paço J, Ferreira A, Tavares J, Jorge RN. The influence of muscles activation on dynamical behavior of the tympano-ossicular system of the middle ear. *Computer Methods in Biomechanics and Biomedical Engineering* 2013; **16**(4):392–402.
38. Gentil F, Jorge RMN, Ferreira AJM, Parente MPL, Moreira M, Almeida E. Estudo do efeito do atrito no contacto entre os ossículos do ouvido médio. *Revista Internacional de Métodos Numéricos para Cálculo y Diseño en Ingeniería* 2007; **23**(2):177–187.
39. Ebnesajjad S. *Fluoroplastics. Non-melt Processible Fluoroplastics,* (1). William Andrew Publishing: Norwich, NY, 2000.
40. Niinomi M. Mechanical properties of biomedical titanium alloys. *Materials Science and Engineering A* 1998; **243**(1–2):231–236.
41. Beer F, Johnston ER, DeWolf J, Mazurek D. *Mechanics of Materials* (6edition). McGraw-Hill Science, 2011.
42. Martins JAC, Pires EB, Salvado R, Dinis PB. A numerical model of passive and active behaviour of skeletal muscles. *Computer Methods in Applied Mechanics and Engineering* 1998; **151**:419–433.
43. Parente MPL, Natal RM, Mascarenhas T, Fernandes AA, Martins JAC. The influence of the material properties on the biomechanical behavior of the pelvic floor muscles during vaginal delivery. *Journal of Biomechanics* 2009; **42**(9):1301–1306. DOI: 10.1016/j.jbiomech.2009.03.011.
44. Humphrey JD, Yin FCP. On constitutive relations and finite deformations of passive cardiac tissue: a pseudostrain-energy function. *Journal of Biomechanical Engineering* 1987; **109**:298–304.
45. Kurokawa H, Goode RL. Sound pressure gain produced by the human middle ear. *Otolaryngology – Head and Neck Surgery* 1995; **113**(4):349–355.
46. Massey BL, Kennedy RJ, Shelton C. Stapedectomy outcomes: titanium versus teflon wire prosthesis. *Laryngoscope* 2005; **115**(2):249–52.
47. Lippy WH, Burkey JM, Schuring AG, Berenholz LP. Comparison of titanium and Robinson stainless steel stapes piston prostheses. *Otology & Neurotology* 2005; **26**(5):874–877.
48. Cotulbea S, Marin AH, Karina M, Ruja AS, Nikolae B. Stapedotomy with implantation of the fisch-type 0.4 mm titanium stapes prosthesis, a good alternative in stapes surgery, 2009. Acta Facultatis Medicae Naissensis.